Revision 1

Nazarovite, $Ni_{12}P_5$, a new terrestrial and meteoritic mineral structurally related to nickelphosphide, Ni_3P

Sergey N. Britvin[1,2]*, Mikhail N. Murashko[1], Maria G. Krzhizhanovskaya[1], Oleg S. Vereshchagin[1], Yevgeny Vapnik[3], Vladimir V. Shilovskikh[4], Maksim S. Lozhkin[5], and Edita V. Obolonskaya[6]

[1] Institute of Earth Sciences, St. Petersburg State University, Universitetskaya Nab. 7/9, 199034 St. Petersburg, Russia

[2] Kola Science Center, Russian Academy of Sciences, Fersman Str. 14, 184200 Apatity, Russia

[3] Department of Geological and Environmental Sciences, Ben-Gurion University of the Negev, P.O.B. 653, Beer-Sheva 84105, Israel

[4] Centre for Geo-Environmental Research and Modeling, St. Petersburg State University, Ulyanovskaya ul. 1, 198504 St. Petersburg, Russia

[5] Nanophotonics Resource Centre, St. Petersburg State University, Ulyanovskaya ul. 1, 198504 St. Petersburg, Russia

[6] The Mining Museum, Saint Petersburg Mining University, 2, 21st Line, 199106 St. Petersburg, Russia

Abstract

Nazarovite, $Ni_{12}P_5$, is a new natural phosphide discovered on Earth and in meteorites. Terrestrial nazarovite originates from phosphide assemblages confined to pyrometamorphic suite of the Hatrurim Formation (the Mottled Zone), the Dead Sea basin, Negev desert, Israel. Meteoritic nazarovite was identified among Ni-rich phosphide precipitates extracted from the Marjalahti meteorite (main group pallasite). Terrestrial mineral occurs as micrometer-sized lamella intergrown with transjordanite (Ni_2P). Meteoritic nazarovite forms chisel-like crystals up to 8 μm long. The mineral is tetragonal, space group $I\bar{4}m$. The unit-cell parameters of terrestrial and meteoritic material, respectively: a 8.640(1) and 8.6543(3), c 5.071(3) and 5.0665(2) Å, V 378.5(2) and 379.47(3) Å^3, $Z = 2$. Crystal structure of terrestrial nazarovite was solved and refined on the basis of X-ray single-crystal data ($R_1 = 0.0516$), whereas the structure of meteoritic mineral was refined by the Rietveld method using an X-ray powder diffraction profile ($R_B = 0.22$ %). The mineral is structurally similar to phosphides of schreibersite–nickelphosphide join, Fe_3P–Ni_3P. Chemical composition of nazarovite (terrestrial/meteoritic, electron microprobe, wt.%): Ni 81.87/78.59, Fe <0.2/4.10; Co <0.2/0.07, P 18.16/17.91, Total 100.03/100.67, leading to the empirical formula $Ni_{11.97}P_{5.03}$ and $(Ni_{11.43}Fe_{0.63}Co_{0.01})_{12.07}P_{4.94}$, based on 17 atoms per formula unit. Nazarovite formation in nature, both on Earth and in meteorites, is related to the processes of Fe/Ni fractionation in solid state, at temperatures below 1100 °C.

Keywords: $Ni_{12}P_5$, nickelphosphide, Fe–Ni–P system, crystal structure, pyrometamorphism, meteorite, planetary interiors, nanoprecipitates

Introduction

Natural phosphides belonging to the ternary system Fe–Ni–P serve as a reservoir of reduced (i.e., non-phosphate) phosphorus in the Solar System (Goldstein et al. 2009; Britvin et al. 2015; Litasov and Shatskiy, 2016). In material science, the crystal chemistry of Fe–Ni phosphides is the foundation for the development of advanced photocatalysts and electrocatalysts (Sun et al. 2016; Sun et al. 2019). In spite of a seemingly compositional simplicity, Fe–Ni–P is a quite complex multiphase field which can be divided into Fe–P and Ni–P subsystems (Table 1). Iron (Z = 26) and nickel (Z = 28) are near-neighbour transition metals, but their phosphides exhibit substantially different chemistry and crystal chemistry (Table 1). The crystal-chemical misfits result in unexpectedly restricted Fe/Ni substitutions. In fact, the joins Fe_3P–Ni_3P (schreibersite–nickelphosphide) and Fe_2P–Ni_2P (barringerite–transjordanite) are the only examples of continuous Fe–Ni solid solutions (Britvin et al. 2020a, 2021a). A limited Fe–Ni miscibility was reported in murashkoite (Vereshchagin et al. 2021), zuktamrurite, allabogdanite (Britvin et al. 2019b) and melliniite, whereas other phosphides do not show traceable Fe/Ni substitutions. The phenomenon of limited miscibility opens a way to crystal-chemical Fe/Ni fractionation within reduced systems. We herein report a new natural phosphide, an extreme example of such fractionation. The mineral $Ni_{12}P_5$ is named nazarovite, in honour of Michail Alexandrovich Nazarov (1949–2016), Russian mineralogist and petrologist, for his contributions to the research of reduced meteoritic assemblages (e.g., Anand et al., 2004; Nazarov et al. 2009). Both the mineral and its name have been approved by the Commission on New Minerals, Nomenclature and Classification, International Mineralogical Association (IMA 2019-013). The holotype specimen of nazarovite from the Hatrurim basin is deposited in the collection of the Fersman Mineralogical Museum, Russian Academy of Sciences, Moscow, Russia, with the registration number 5381/1.

This is the peer-reviewed, final accepted version for American Mineralogist, published by the Mineralogical Society of America.
The published version is subject to change. Cite as Authors (Year) Title. American Mineralogist, in press.
DOI: https://doi.org/10.2138/am-2022-8219. http://www.minsocam.org/

Samples and methods

Terrestrial nazarovite (the holotype material)

The mineral was discovered among phosphide assemblages confined to the rocks of the Hatrurim Formation (the Mottled Zone) – a huge pyrometamorphic complex spanning the Middle East in Israel, West Jordan and West Bank (Gross 1977; Vapnik et al. 2007; Novikov et al. 2013). Nazarovite occurs in the specimens of altered diopside microbreccia collected along the Halamish wadi, Hatrurim basin, Negev desert, Israel (e.g., Britvin et al. 2021b). It was studied in conventional polished thick rock sections.

Nazarovite from the Marjalahti pallasite

An acid-resistant precipitate was obtained from a piece of the metal taken from the same meteorite slice where keplerite, $Ca_9(Ca_{0.5}\square_{0.5})Mg(PO_4)_7$, was recently described (specimen MM74/2, the Mining Museum) (Britvin et al. 2021d). A ~0.5 cm (Fe,Ni) metal chunk, free of olivine and chromite rims, was preliminarily treated in hot 10 % HCl for 1 minute, in order to clean it up from surface contaminants. The etched piece was rinsed off by distilled water and then immersed into 10 mL of hot 10 % HCl, in 50 mL glass baker on a hot plate. After complete dissolution of acid-soluble α-(Fe,Ni) (kamacite), the liquid with the insoluble residue was mixed with ~30 mL of methanol and allowed to stay for 20 min, followed by gentle removal of the solution with a 20 mL syringe until ~1 cm level of residual liquid remained. This wash-up procedure was repeated 5 times, and after that the remaining liquid with precipitate was transferred onto a watch glass and air-dried. The residue was comprised by a few mm-sized grains of schreibersite, $(Fe,Ni)_3P$, and taenite, γ-(Fe,Ni). In addition, a tiny film of white color with straw-yellowish tint and metallic luster was observed at the bottom of the glass. It was found that the film is a microgranular phosphide precipitate which was harvested into a drop of epoxy resin. The soft acid treatment of meteoritic iron applied herein follows the method used in the metallurgy for the liberation of phosphide precipitates from the Ni-

based alloys (e.g., Lee et al., 1996). It is noteworthy that this procedure does not lead to the appearance of new phosphide phases, therefore nazarovite is not a newly formed phosphide. The obtained phosphide precipitate sample was first subjected to X-ray powder diffraction study and later on, after embedding and polishing procedures, to electron microprobe analysis.

Electron microprobe analysis (EMPA) and electron backscatter diffraction (EBSD)

EMPA data were obtained using an Oxford Instruments AzTec Energy X-Max 20 EDX spectrometer (20 kV, 1 nA) attached to a Hitachi S-3400N SEM. Cobalt was determined separately using an INCA WAVE 500 WDX spectrometer (20 kV, 15 nA). Pure Ni, Fe and Co metals, along with InP were used as standards. Electron backscatter diffraction (EBSD) mapping was carried out on the section etched for 20 min with an Ar-ion beam generated by an Oxford Instruments IonFab-300 instrument. Diffraction pattern acquisition was carried out with an Oxford Instruments Nordlys-HKL detector operated at 30 kV and 1.5 nA on the sample coated with ~2 nm carbon film and glued onto a 70 ° tilted stage. The EBSD patterns matching and mapping were performed using the structural models of $Ni_{12}P_5$ (Rundqvist and Larsson 1959) and transjordanite end-member, Ni_2P (Britvin et al. 2020a).

Powder X-ray diffraction (PXRD) and Rietveld refinement

Powder diffraction patterns were obtained by the use of a Rigaku RAXIS Rapid II diffractometer (Table 2). The instrument has a Co*K*α-radiation source (rotating anode, 40 kV, 15 mA), microfocus mirror monochromator and semi-cylindrical imaging plate detector (r = 127.4 mm). The images were acquired in Debye-Scherrer geometry (Gandolfi-type rotation). A plate-to-profile data conversion was performed with the osc2xrd program (Britvin et al. 2017). Further processing of the pattern of the terrestrial nazarovite-transjordanite grain was carried out with Stoe WinXPOW software (Stoe and Cie GmbH). Rietveld refinement of the powder profile obtained

from the meteoritic precipitate (Supplementary Fig. S1) was carried out with Bruker TOPAS v.5.0 software (Bruker AXS). The basic refinement details and refined fractional coordinates are given in Supplemental Tables S1 and S2.

Single-crystal X-ray diffraction (SCXRD)

SCXRD data were obtained only for terrestrial nazarovite; they were collected by means of a Bruker Kappa APEX DUO diffractometer (1024K CCD detector). The crystal used for the study is depicted in Figure 1. Because of the small size of nazarovite lamella, we did not extract them from the surrounding transjordanite matrix. Instead, the whole two-phase grain was subjected to data collection. A single-crystal nazarovite domain (UB-matrix) could be separated from several transjordanite UB-matrices using CrysAlisPro software (Rigaku Oxford Diffraction), followed by a standard set of data reduction procedures. The crystal structure of terrestrial nazarovite was solved and refined to $R_1 = 0.0516$ using the *SHELX*-2018 set of programs (Sheldrick 2015) incorporated into Olex2 GUI (Dolomanov et al. 2006). A summary of data collection and structure refinement details is given is Supplementary Table 3. The detailed information can be retrieved from the CIF file attached to Supplementary Data.

Results

Occurrence and general appearance

Microcrystalline diopside constitutes up to 80 % of microbreccia containing phosphide minerals, whereas the interstices are filled with secondary thaumasite, ettringite and unidentified Mg-Fe hydrous silicates. The accessory minerals are comprised by hematite, magnetite, and diverse Fe-Ni phosphides (Britvin et al. 2021c). Nazarovite occurs as single-crystal lamella up to 10 μm long penetrating the grain of transjordanite, Ni_2P (Fig. 1). EBSD mapping reveals that all nazarovite lamella exposed onto the section surface have the same crystallographic orientation, whereas

surrounding transjordanite forms a patchy polycrystalline aggregate (Fig. 1d-f). Nazarovite-transjordanite intergrowths have white colour in reflected light; both minerals are indistinguishable from each other under the polarizing microscope. Due to very small size of nazarovite lamella, the microhardness and reflectance values of the mineral could not be measured.

Nazarovite of meteoritic origin was identified in microgranular precipitates obtained by dissolution of α-(Fe,Ni) metal (kamacite) of the Marjalahti meteorite (main-group pallasite). The dominant phase of precipitates is acicular to thin-prismatic nickelphosphide, $(Ni,Fe)_3P$, which accounts for 85-90 wt.% of acid-resistant residue (Supplementary Fig. S1). Nazarovite occurs as chisel-like crystals up to 8 μm wide and 3 μm thick disseminated among nickelphosphide (Fig. 2).

Crystal structure

The unit-cell parameters of terrestrial and meteoritic nazarovite are almost identical, in agreement with the composition approaching pure $Ni_{12}P_5$ (Table 3). The crystal structure of the mineral contains 2 independent Ni positions and 2 P sites (Table 4). The Ni(1) atom is coordinated by 12 atoms – 5Ni(1), 3Ni(2), 3P(1), and 1P(2). Ni(2) has 15-fold coordination – by 6Ni(1), 5Ni(2), and 4P(1). Phosphorus atoms, P(1) and P(2), are surrounded solely by Ni and have coordination numbers 10 and 8, respectively. Due to a relative simplicity of the P-centered polyhedra, the nazarovite structure can be better illustrated in a phosphorus-centered approach (Fig. 3), in contrast to the early descriptions of synthetic $Ni_{12}P_5$ based on the metal-centered polyhedra (Rundqvist and Larsson 1959; Larson 1965). The nazarovite framework (Fig. 3a,b) is topologically similar to that of the minerals belonging to schreibersite–nickelphosphide join, Fe_3P–Ni_3P (Britvin et al. 2021a). Both nazarovite and nickelphosphide are tetragonal, have very similar lattice metrics (Table 3), and the relationship between their unit-cell contents can be expressed as $2\times Ni_{12}P_5$ ($Ni_{24}P_{10}$) ↔ $8\times Ni_3P$ ($Ni_{24}P_8$). It can be seen that the nazarovite cell contains by 2 P atoms more than that of nickelphosphide. These additional P(2) atoms are inserted approximately into the positions which

are vacant in the structure of nickelphosphide (Fig. 3). The P(2) coordination polyhedron of nazarovite represents an almost perfect cube [PNi_8]. The introduction of [PNi_8] cubes into the lattice results in its symmetrization, manifested by the conversion from the space group $I\bar{4}$ (Ni_3P) to $I4/m$ ($Ni_{12}P_5$). The additional effect of phosphorus incorporation is a relative stretching of the lattice along the *c*-axis that is manifested in the increase of the *c*/*a* ratio (Table 3).

Chemical composition

The appearance of an additional P(2) site in nazarovite (relative to nickelphosphide) results in the abrupt decrease of the structural tolerance towards Fe substitution. As was already mentioned, Ni_3P (nickelphosphide) forms a continuous series of solid solutions with Fe_3P (schreibersite) (Table 1). In contrast, both occurrences of nazarovite show the compositions either approaching or exactly matching end-member $Ni_{12}P_5$ (Table 5). The marked difference in the affinity of respective phosphides towards Fe is illustrated by the comparison of both minerals from the Marjalahti pallasite, where nazarovite has a Ni/Fe ratio of more than 18, whereas the same ratio in nickelphosphide is just 2 (Table 5). Such a difference is not an occasional one, but is supported by the studies on synthetic systems: $Fe_{12}P_5$ does not exist in the Fe–P phase diagram, and Fe does not substitute for Ni in synthetic $Ni_{12}P_5$ (Drábek 2006). Therefore, the extreme Ni enrichment of natural nazarovite can be considered as its intrinsic property rather than a geochemical curiosity.

Discussion

Nazarovite is an example of the influence of crystal-chemical factors on the elemental differentiation in the Fe–Ni–P system. In both terrestrial and meteoritic environments, the mineral was evidently formed in the solid state at temperatures below 1100 °C, as it can be deduced from the studies of the Ni–P phase diagram (Schmetterer et al. 2009). The results of EBSD and X-ray single-crystal study suggest that spatially separated nazarovite lamellae shown in Figure 1 represent the

subdomains (the remnants?) of the same single crystal. The latter implies that nazarovite may in fact be a primary, earlier phase in the assemblage, whereas surrounding patchy transjordanite is a subsequent one, possibly formed via solid-state substitution of nazarovite.

The Marjalahti is one of a few witnessed pallasite falls (see a historical summary in Britvin et al. 2021d). The fragments of this meteorite, harvested immediately after the fall, were not affected by terrestrial weathering; thereby nazarovite in the Marjalahti has a cosmic origin, rather than being a product of surficial alteration of schreibersite $(Fe,Ni)_3P$, as it was discussed with respect to barringerite, $(Fe,Ni)_2P$ (Buseck 1969; Britvin et al. 2020a). The identification of nazarovite in phosphide assemblages is hampered due to its compositional similarity to nickelphosphide, $(Ni,Fe)_3P$, and transjordanite, $(Ni,Fe)_2P$. However, there is evidence that this phosphide may be more widespread in nature. Armstrong et al. (1987) described mm-sized fremdlinge (sulphide- and metal-rich droplets) within the B-type calcium-aluminium inclusion (CAI) of the Allende meteorite, a CV3 carbonaceous chondrite. Among other opaque phases, Armstrong et al. (1987) reported a Ni phosphide containing 80–81 wt.% Ni and less than 0.5 wt.% Fe. The authors calculated a phosphide formula of Ni_5P_2, but the assumed ideal Ni/P atomic ratio of 2.5 is quite close to that of 2.4 in nazarovite (Table 1). Garvie (2019) described Ni-rich phosphide nanoprecipitates from the Odessa octahedrite, containing both nickelphosphide (the major phase) and the second phosphide that can be attributed to either $Ni_{12}P_5$ (i.e., nazarovite) or Ni_8P_3. Taking into account that Odessa belongs to the most common IAB group of iron meteorites whereas Marjalahti is a typical main-group pallasite, we propose that the similar Ni-rich phosphide precipitates can be extracted from acid-resistant residues of many metal-rich meteorites.

Implications

The study of natural Ni and Fe phosphides expands our knowledge of the phase relations within Fe-Ni metal-rich assemblages, which are thought to constitute planetary interiors of celestial

220 bodies. The presence of nazarovite determines the upper thermal limit of 1100 °C for the formation
221 of its assemblages, and opens the opportunities for determination of pressure stability limits. The
222 influence of crystal-chemical factors on the processes of elemental differentiation in reduced
223 systems is a largely obscure field of mineralogy and geochemistry. Here the most prominent is the
224 Fe-Ni system (e.g., Goldstein et al. 2009), where the formation of γ-(Fe,Ni) (taenite) succeeds in
225 further selective enrichment of this phase in Ni relative to coexisting α-(Fe,Ni) (kamacite). The
226 much less studied are Fe-Ni carbide systems, where haxonite, $(Fe,Ni)_{23}C_6$, is always and
227 considerably enriched in Ni as compared to cohenite, $(Fe,Ni)_3C$ (Krot et al. 1997; Scott and
228 Goldstein 2012), but the reason for such a behavior is unclear. Among natural phosphides, one can
229 mention the selective affinity of Co towards allabogdanite, the high-pressure modification of
230 $(Fe,Ni)_2P$ (Britvin et al. 2019b). The present paper contributes to this area of planetary science, at
231 the junction between crystal chemistry and cosmochemistry. From the methodological point of
232 view, this study illustrates how advances in the X-ray instrumentation enhance the quality of crystal-
233 chemical research, in particular in meteoritics and planetary science. The full-scale structural study
234 of μm-sized mineral grains is now achievable using standard in-house instruments – a step toward
235 complementary to the fingerprint techniques like EBSD and the Laue X-ray method.
236

237 **Acknowledgments**

238 This study was funded by the Russian Science Foundation, grant 18-17-00079. The authors are
239 indebted to the curators of the Mining Museum, St. Petersburg Mining Institute, for the specimen of
240 the Marjalahti pallasite provided for this study. We gratefully acknowledge the referees, Laurence
241 Garvie and Michael Zolensky, for helpful comments and suggestions, and the Technical Editor for
242 the crystallographic data corrections. This paper has benefited from editorial handling by Daniel
243 Hummer. The authors are thankful to the X-ray Diffraction Centre, Centre for Microscopy and

244 Microanalysis, Nanophotonics, Nanotechnology and Geomodel Resource Centres of St. Petersburg
245 State University for the access to instrumental and computational resources.

246

247 **References cited**

248 Anand, M., Taylor, L.A., Nazarov, M.A., Shu, J., Mao, H.-K., and Hemley, R.J. (2004) Space
249 weathering on airless planetary bodies: Clues from the lunar mineral hapkeite. Proceedings of
250 the National Academy of Sciences of the United States of America, 101, 6847–6851.
251 Armstrong, T., Hutcheon, I.D., and Wasserburg, G.J. (1987) Zelda and company: petrogenesis of
252 sulfide-rich Fremdlinge and constraints on solar nebula processes. Geochimica et
253 Cosmochimica Acta, 51, 3155–3173.
254 Britvin, S.N., Kolomensky, V.D., Boldyreva, M.M., Bogdanova, A.N., Kretser, Yu.L., Boldyreva,
255 O.N., and Rudashevskii, N.S. (1999) Nickelphosphide, $(Ni,Fe)_3P$, the nickel analog of
256 schreibersite. Proceedings of Russian Mineralogical Society, 128, 64–72 (in Russian).
257 Britvin, S.N., Murashko, M.N., Vapnik, Ye., Polekhovsky, Yu.S., and Krivovichev, S.V. (2015)
258 Earth's phosphides in Levant and insights into the source of Archaean prebiotic phosphorus.
259 Scientific Reports, 5, 8355.
260 Britvin, S.N., Dolivo-Dobrovolsky, D.V., Krzhizhanovskaya, M.G. (2017) Software for processing
261 the X-ray powder diffraction data obtained from the curved image plate detector of Rigaku
262 RAXIS Rapid II diffractometer. Zapiski Rossiyskogo Mineralalogicheskogo Obshchestva,
263 146, 104–107 (in Russian).
264 Britvin, S.N., Murashko, M.N., Vapnik, Ye., Polekhovsky, Yu.S., Krivovichev, S.V., Vereshchagin,
265 O.S., Vlasenko, N.S., Shilovskikh, V.V., and Zaitsev, A.N. (2019a) Zuktamrurite, FeP_2, a new
266 mineral, the phosphide analogue of löllingite, $FeAs_2$. Physics and Chemistry of Minerals, 46,
267 361–369.

Britvin, S.N., Shilovskikh, V.V., Pagano, R., Vlasenko, N.S., Zaitsev, A.N., Krzhizhanovskaya, M.G., Lozhkin, M.S., Zolotarev, A.A., and Gurzhiy, V.V. (2019b) Allabogdanite, the high-pressure polymorph of $(Fe,Ni)_2P$, a stishovite-grade indicator of impact processes in the Fe–Ni–P system. Scientific Reports, 9, 1047.

Britvin, S.N., Vapnik, Ye., Polekhovsky, Yu.S. and Krivovichev, S.V., Krzhizhanovkaya M.G., Gorelova L.A., Vereshchagin, O.S., Shilovskikh, V.V., and Zaitsev, A.N. (2019c) Murashkoite, FeP, a new terrestrial phosphide from pyrometamorphic rocks of the Hatrurim Formation, Southern Levant. Mineralogy and Petrology, 113, 237–248.

Britvin, S.N., Murashko, M.N., Vapnik, Ye., Polekhovsky, Yu.S., Krivovichev, S.V., Krzhizhanovskaya, M.G., Vereshchagin, O.S., Shilovskikh, V.V., and Vlasenko, N.S. (2020a) Transjordanite, Ni_2P, a new terrestrial and meteoritic phosphide, and natural solid solutions barringerite–transjordanite (hexagonal Fe_2P–Ni_2P). American Mineralogist, 105, 428–436.

Britvin, S.N., Murashko, M.N., Vapnik, Ye., Polekhovsky, Yu.S., Krivovichev, S.V., Vereshchagin, O.S., Shilovskikh, V.V., Vlasenko, N.S., and Krzhizhanovskaya, M.G. (2020b) Halamishite, Ni_5P_4, a new terrestrial phosphide in the Ni–P system. Physics and Chemistry of Minerals, 2020, 3.

Britvin, S.N., Murashko, M.N., Vapnik, Ye., Polekhovsky, Yu.S., Krivovichev, S.V., Vereshchagin, O.S., Shilovskikh, V.V., and Krzhizhanovskaya, M.G. (2020c) Negevite, the pyrite-type NiP_2, a new terrestrial phosphide. American Mineralogist, 105, 422–427.

Britvin, S.N., Krzhizhanovskaya, M.G., Zolotarev, A.A., Gorelova, L.A., Obolonskaya, E.V., Vlasenko, N.S., Shilovskikh, V.V., and Murashko, M.N. (2021a) Crystal chemistry of schreibersite, $(Fe,Ni)_3P$. American Mineralogist, 106, 10.2138/am-2021-7766

Britvin, S.N., Murashko, M.N., Vapnik ,Ye., Vlasenko, N.S., Krzhizhanovskaya, M.G., Vereshchagin, O.S., Bocharov, V.N., and Lozhkin, M.S. (2021b) Cyclophosphates, a new

class of native phosphorus compounds, and some insights into prebiotic phosphorylation on early Earth. Geology, 49, 382–386.

Britvin, S.N., Vereshchagin, O.S., Shilovskikh, V.V., Krzhizhanovskaya, M.G., Gorelova, L.A., Vlasenko, N.S., Pakhomova, A.S., Zaitsev, A.N., Zolotarev, A.A., Bykov, M., Lozhkin, M.S., and Nestola, F. (2021c) Discovery of terrestrial allabogdanite $(Fe,Ni)_2P$, and the effect of Ni and Mo substitution on the barringerite-allabogdanite high-pressure transition. American Mineralogist, 106, 944–952.

Britvin, S.N., Galuskina, I.O., Vlasenko, N.S., Vereshchagin, O.S., Bocharov, V.N., Krzhizhanovskaya, M.G., Shilovskikh, V.V., Galuskin, E.V., Vapnik, Ye., and Obolonskaya, E.V (2021d) Keplerite, $Ca_9(Ca_{0.5}\square_{0.5})Mg(PO_4)_7$, a new meteoritic and terrestrial phosphate isomorphous with merrillite, $Ca_9NaMg(PO_4)_7$. American Mineralogist, 106, 10.2138/am-2021-7834

Buseck, P.R. (1969) Phosphide from meteorites: Barringerite, a new iron-nickel mineral. Science, 165, 169–171.

Dolomanov, O.V., Bourhis, L.J., Gildea, R.J., Howard, J.A., and Puschmann, H. (2009) OLEX2: a complete structure solution, refinement and analysis program. Journal of Applied Crystallography, 42, 339–341.

Dowty, E. (2006). ATOMS for Windows. Shape Software, Kingsport, Tennessee, USA.

Drábek, M. (2006) Phosphide solid-solutions within the metal-rich portion of the quaternary system Co–Fe–Ni–P AT 800°C, and mineralogical implications. Canadian Mineralogist, 44, 399–408.

Garvie, L.A.J. Germanium- and gallium-rich nickel phosphide "Ni_3P" nanoprecipitates from the Odessa (IAB-MG) iron meteorite. 50th Lunar and Planetary Science Conference, Abstract #2639.

Goldstein, J.I., Scott, E.R.D., and Chabot, N.L. (2009) Iron meteorites: Crystallization, thermal history, parent bodies, and origin. Chemie der Erde, 69, 293–325.

317 Gross, S. (1977) The mineralogy of the Hatrurim Formation, Israel. Geological Survey of Israel
318 Bulletin, 70, 1–80.
319 Ilnitskaya, O.N., Akselrud, L.G., Mikhalenko, S.I., and Kuzma, Yu.B. (1987) Crystal structure of
320 alpha-Ni_8P_3. Kristallografiya, 32, 50–54 (in Russian).
321 Jeitschko, W., and Braun, D.J. (1978) Synthesis and crystal structure of the iron polyphosphide
322 FeP_4. Acta Crystallographica, B34, 3196–3201.
323 Krot, A.N., Zolensky, M.E., Wasson, J.T., Scott, E.R.D., Keil, K., and Ohsumi, K. (1997) Carbide
324 magnetite assemblages in type 3 ordinary chondrites. Geochimica et Cosmochimica Acta, 61,
325 219–237.
326 Larsson, E. (1965) An X-ray investigation of the Ni-P system and the crystal structures of NiP and
327 NiP_2. Arkiv för Kemi, 23, 335–365.
328 Lee, H.-J., Akiyama, E., Habazaki, H., Kawashima, A., Asami, K., and Hashimoto, K. (1996) The
329 effect of phosphorus addition on the corrosion behavior of arc-melted Ni-10Ta-P alloys in 12
330 M HCl. Corrosion Science, 38, 469–485.
331 Litasov, K., and Shatskiy, A. (2016) Composition of the Earth's core: a review. Russian Geology
332 and Geophysics, 57, 22–46.
333 Nazarov, M.A., Kurat, G., Brandstaetter, F., Ntaflos, T., Chaussidon, M., and Hoppe, P. (2009)
334 Phosphorus-bearing sulfides and their associations in CM chondrites. Petrology, 17, 101–123.
335 Novikov, I., Vapnik, Ye., and Safonova, I. (2013) Mud volcano origin of the Mottled Zone,
336 Southern Levant. Geoscience Frontiers, 4, 597–619.
337 Oryshchyn, S., Babizhetskii, V.S., Chikhrii, S.I., Akselrud, L.G., Stojko, S., Bauer, D., Guerin, P.,
338 and Kuzma, Yu.B. (2004) Crystal structure of Ni_5P_2. Neorganicheskie Materialy, 40, 450–456
339 (in Russian).

Pratesi, G., Bindi, L., and Moggi-Cecci, V. (2006) Icosahedral coordination of phosphorus in the crystal structure of melliniite, a new phosphide mineral from the Northwest Africa 1054 acapulcoite. American Mineralogist, 91, 451–454.

Rundqvist, S., and Ersson, N.O. (1969) Structure and bonding in skutterudite-type phosphides. Arkiv för Kemi, 30, 103–115.

Rundqvist, S., and Larsson, E. (1959) The crystal structure of $Ni_{12}P_5$. Acta Chemica Scandinavica, 13, 551–560.

Schmetterer, C., Vizdal, J., and Ipser, H. (2009) A new investigation of the system Ni–P. Intermetallics, 17, 826–834.

Scott, E.R.D., and Goldstein, J.I. (2012) Occurrence of carbides and graphite in iron meteorites and origin of C-rich irons. Lunar Planetary Science, 43, #2671 (abstract).

Sheldrick, G.M. (2015) Crystal structure refinement with *SHELXL*. Acta Crystallographica, C71, 3–8.

Skála, R., and Drábek, M. (2003) Nickelphosphide from the Vicenice octahedrite: Rietveld crystal structure refinement of a synthetic analogue. Mineralogical Magazine, 67, 783–792.

Sugitani, M., Kinomura, N., Koizumi, M., and Kume, S. (1978) Preparation and properties of a new iron phosphide FeP_4. Journal of Solid State Chemistry, 26, 195–201.

Sun, M., Liu, H., Qu, J., and Li, J. (2016) Earth-Rich Transition Metal Phosphide for Energy Conversion and Storage. Advanced Energy Materials, 6, 1600087.

Sun, Z., Zhu, M., Lv, X., Liu, Y., Shi, C., Dai, Y., Wang, A, and Majima, T. (2019) Insight into Iron Group Transition Metal Phosphides (Fe_2P, Co_2P, Ni_2P) for Improving Photocatalytic Hydrogen Generation. Applied Catalysis B: Environmental, 246, 330–336.

Vapnik, Ye., Sharygin, V.V., Sokol, E.V., and Shagam, R. (2007) Paralavas in a combustion metamorphic complex: Hatrurim Basin, Israel. The Geological Society of America, Reviews in Engineering Geology, 18, 133–153.

365 Vereshchagin, O.S., Pankin, D.V., Smirnov, M.B., Vlasenko, N.S., Shilovskikh, V.V., and Britvin,
366 S.N. (2021) Raman spectroscopy: A promising tool for the characterization of transition metal
367 phosphides. Journal of Alloys and Compounds, 853, 156468.

368 **List of figure captions**

369

370 **Figure 1.** Nazarovite in the phosphide assemblage of the Hatrurim Basin. (a) Polished section in
371 reflected light. Phosphide grain within the weathered silicate paralava. (b) The same grain, BSE
372 image with enhanced contrast. A series of tiny nazarovite lamellae (light) penetrate transjordanite
373 matrix. The biggest lamella was used for the structure solution and refinement. (c) EBSD phase map
374 of the same grain (nazarovite is yellow, transjordanite is green). (d) EBSD map in inverse pole
375 figure (IPF) colouring. Note that all nazarovite lamellae (blue) are represented by single crystals,
376 whereas encasing transjordanite forms a polycrystalline aggregate (patchy areas). (e) EBSD pole
377 figure of nazarovite in the area depicted in (d), projection onto {001}. Note that all nazarovite
378 lamellae have coincident crystallographic orientation, with the *c*-axis approximately parallel to the
379 image plane. (f) EBSD pole figure of transjordanite in the same area – a polycrystal consisting of at
380 least 3 randomly oriented domains. Abbreviations: Nz – nazarovite, Tj – transjordanite (Ni_2P), Mgt
381 – magnetite.

382

383 **Figure 2.** Nazarovite crystal (Nz) among an aggregate of nickelphosphide crystals. Polished section
384 of acid-resistant precipitate encapsulated into epoxy resin. SEM BSE image. The Marjalahti
385 pallasite.

386

387 **Figure 3.** Crystal structures of nazarovite, $Ni_{12}P_5$, and nickelphosphide, Ni_3P, in a phosphorus-
388 centered representation. (a) Nazarovite, a slice on (001). Framework of edge-sharing P(1)-centered
389 polyhedra [PNi_{10}] (yellow) and perfect P(2)-centered cubes [PNi_8] (green). (b) A cut of the
390 nazarovite framework illustrating the alternation of [PNi_8] and empty [$\square Ni_8$] cubes interleaved along
391 the *c*-axis. (c) Nickelphosphide, a slice on (001) in the same orientation as of nazarovite. A

framework of edge-sharing polyhedra [$P(Ni_7P_2)$], with the narrow open channels propagating along the *c*-axis. Drawn in ATOMS v.6 (Dowty 2006).

This is the peer-reviewed, final accepted version for American Mineralogist, published by the Mineralogical Society of America.
The published version is subject to change. Cite as Authors (Year) Title. American Mineralogist, in press.
DOI: https://doi.org/10.2138/am-2022-8219. http://www.minsocam.org/

Tables

Table 1. Juxtaposition of natural and synthetic phosphides in the system Fe–Ni–P [a].

***M*:P atomic ratio**	**Fe–P join**		**Ni–P join**			
	Mineral	**Ideal formula**		**Mineral**	**Struct. type**	**Ref.** [b]
4			Ni_4P	Melliniite	Al_4Au	[1]
3	Schreibersite	Fe_3P	Ni_3P	Nickelphosphide	Ni_3P	[2]
2.67			Ni_8P_3		Ni_8P_3	[3]
2.5			Ni_5P_2		Ni_5As_2	[4]
2.4			$Ni_{12}P_5$	Nazarovite	$Ni_{12}P_5$	[5]
2	Barringerite	Fe_2P	Ni_2P	Transjordanite	Fe_2P	[6]
2	Allabogdanite	Fe_2P	Ni_2P	Orishchinite	Co_2Si	[7]
1.25			Ni_5P_4	Halamishite	Ni_5P_4	[8]
1	Murashkoite	FeP			MnP	[9]
1			NiP		NiP	[10]
0.5	Zuktamrurite	FeP_2			Marcasite	[11]
0.5			NiP_2	Negevite	Pyrite	[12]
0.33			NiP_3		Skutterudite	[13]
0.25		FeP_4			FeP_4	[14]
0.25		FeP_4			CrP_4	[15]

[a] The phases which can exist under ambient conditions (either in stable or in quenched state).
[b]References: [1] Pratesi et al. 2006; [2] Britvin et al. 1999, 2021a; [3] Ilnitskaya et al. 1987; [4] Oryshchyn et al. 2004; [5] This work; [6] Britvin et al. 2020a; [7] Britvin et al. 2021c; [8] Britvin et al. 2020b; [9] Britvin et al. 2019c; [10] Larsson 1965; [11] Britvin et al. 2019a; [12] Britvin et al. 2020c; [13] Rundqvist and Ersson 1969; [14] Jeitschko and Braun 1978; [15] Sugitani et al. 1978.

This is the peer-reviewed, final accepted version for American Mineralogist, published by the Mineralogical Society of America.
The published version is subject to change. Cite as Authors (Year) Title. American Mineralogist, in press.
DOI: https://doi.org/10.2138/am-2022-8219. http://www.minsocam.org/

405

406 Table 2. Powder X-ray diffraction data for nazarovite (*d* in Å)

Hatrurim basin				Marjalahti pallasite				
I_{obs}	d_{obs}	I_{calc}	d_{calc}	I_{obs}	d_{obs}	I_{calc}	d_{calc}	***hkl***
5	4.374	3	4.374	3	4.370	2	4.372	101
		3	4.320					200
		2	3.073	3	3.080	4	3.076	211
		2	3.054	5	3.062	4	3.060	220
		11	2.732	15	2.736	13	2.737	310
5	2.503	9	2.504	8	2.508	6	2.507	301
54	2.341	39	2.342	43	2.339	40	2.341	112
		16	2.187	[b]		18	2.186	202
		17	2.167	[b]		14	2.169	321
13	2.160	23	2.160	[b]		21	2.164	400
15 [a]	2.040	19	2.036	27	2.038	22	2.040	330
		7	1.937			4	1.939	411
40 [a]	1.931	59	1.932	69	1.934	62	1.935	420
100	1.860	100	1.859	100	1.858	100	1.859	312
		7	1.694	10	1.696	8	1.697	510
		3	1.644	5	1.643	3	1.645	402
				5	1.637	6	1.638	501
		8	1.636					431
		3	1.588					332
		5	1.537			8	1.538	422
		2	1.409	5	1.410	4	1.410	512
		3	1.381			3	1.381	323
		5	1.366	6	1.368	5	1.368	620
		9	1.279	[b]		11	1.281	532
		9	1.268	[b]		10	1.267	004
		6	1.222	[b]		9	1.224	710
		3	1.208			2	1.209	433
		13	1.203	14	1.204	18	1.204	622

407

408 [a] The line partially overlaps with the reflection from transjordanite. [b] Line completely
409 overlaps with the reflection from nickelphosphide, $(Ni,Fe)_3P$.
410

411

412 Table 3. Crystal parameters of nazarovite and synthetic end-member nickelphosphide.
413

Mineral	Nazarovite			Nickelphosphide
Locality	Hatrurim	Hatrurim	Marjalahti	Synthetic
Method	SCXRD	PXRD	Rietveld	Rietveld
Formula	$Ni_{12}P_5$	$Ni_{12}P_5$	$(Ni_{11.43}Fe_{0.67})_{12}P_5$	Ni_3P
Space group	*I*4/m	*I*4/m	*I*4/m	$I\bar{4}$
a (Å)	8.640(1)	8.639(5)	8.6543(3)	8.9546(1)
c (Å)	5.071(3)	5.072(3)	5.0665(2)	4.3871(1)
c/*a* ×10	5.869	5.871	5.853	4.899
V (Å^3)	378.5(2)	378.6(6)	379.47(3)	351.78(2)
Z	2	2	2	8
D_x (g cm^{-1})	7.54	7.54	7.55	7.82
Reference	This work	This work	This work	Skála and Drábek 2003

414

415

This is the peer-reviewed, final accepted version for American Mineralogist, published by the Mineralogical Society of America.
The published version is subject to change. Cite as Authors (Year) Title. American Mineralogist, in press.
DOI: https://doi.org/10.2138/am-2022-8219. http://www.minsocam.org/

Table 4. Selected interatomic bond distances (Å) for nazarovite.

Bond	Distance	
	Hatrurim	Marjalahti
Ni1–Ni1	2.522(3)	2.53(2)
Ni1–Ni1	2.549(3)	2.54(2)
Ni1–Ni1	2.587(3)	2.605(10)
Ni1–Ni1	2.639(2) ×2	2.647(7) ×2
Ni1–Ni2	2.540(2)	2.531(10)
Ni1–Ni2	2.574(2)	2.556(10)
Ni1–Ni2	2.705(2)	2.716(10)
Ni1–P1	2.222(3)	2.340(14)
Ni1–P1	2.424(3)	2.350(15)
Ni1–P1	2.455(3)	2.556(15)
Ni1–P2	2.252(1)	2.262(7)
Ni2–Ni2	2.544(4)	2.574(16)
Ni2–P1	2.240(4)	2.083(17)
Ni2–P1	2.242(4)	2.206(19)
Ni2–P1	2.600(2) ×2	2.571(3) ×2

Table 5. Chemical composition (wt. %) of nazarovite and associated phosphides.

	Hatrurim basin		**Marjalahti pallasite**	
	Nazarovite	Transjordanite	Nazarovite	Nickelphosphide
	n = 7 (range)	*n* = 6 (range)	*n* = 4 (range)	*n* = 5 (range)
Ni	81.87 (81.39–82.29)	79.04 (78.26–79.73)	78.59 (78.01–79.42)	59.35 (52.90–63.92)
Fe	< 0.2	< 0.2	4.10 (3.46–5.13)	25.81 (21.22–31.37)
Co	< 0.2	< 0.2	0.07 (0.00–0.29)	0.23 (0.20–0.27)
P	18.16 (18.01–18.35)	21.01 (20.85–21.12)	17.91 (17.52–18.23)	15.01 (14.89–15.21)
Total	100.03	100.05	100.67	100.40
		Formula amounts		
	Σ = 17 *apfu*	Σ = 3 *apfu*	Σ = 17 *apfu*	Σ = 4 *apfu*
Ni	11.97	1.99	11.43	2.06
Fe			0.63	0.94
Co			0.01	0.01
Σ	11.97	1.99	12.07	3.01
P	5.03	1.01	4.94	0.99

This is the peer-reviewed, final accepted version for American Mineralogist, published by the Mineralogical Society of America.
The published version is subject to change. Cite as Authors (Year) Title. American Mineralogist, in press.
DOI: https://doi.org/10.2138/am-2022-8219. http://www.minsocam.org/

435 **Figures**

436

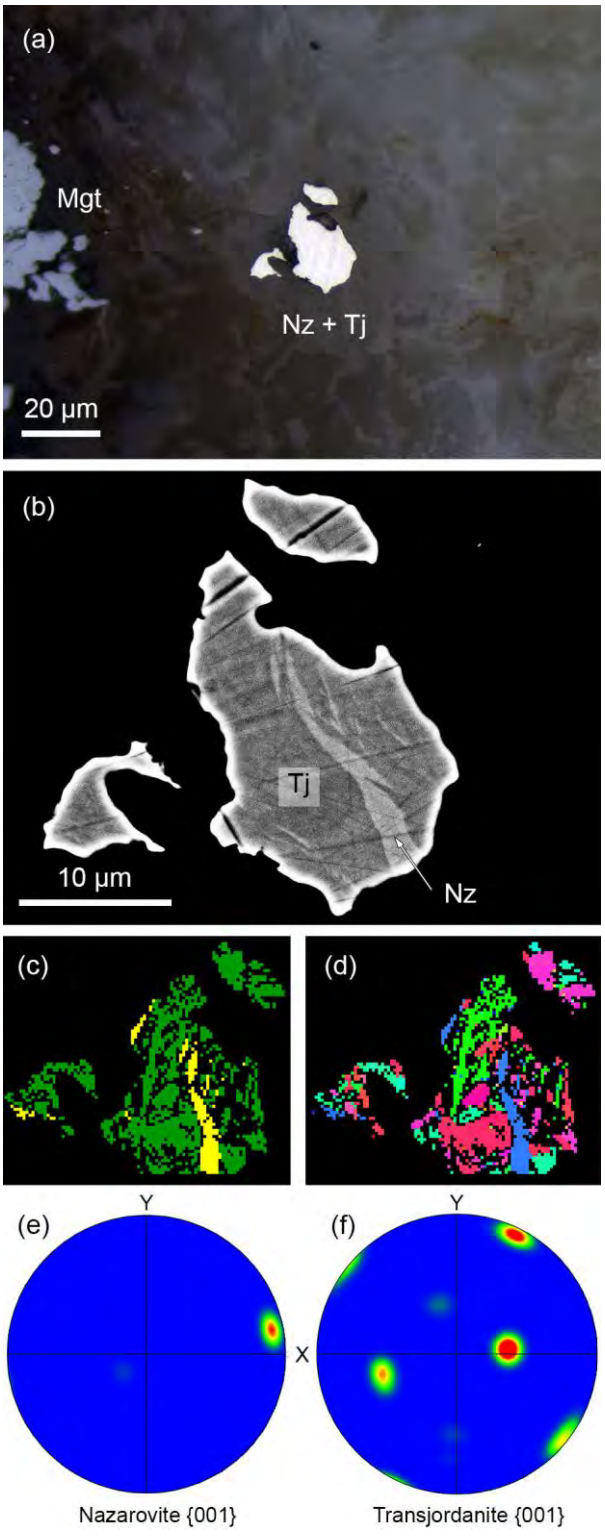

437

438 **Figure 1**

439

440

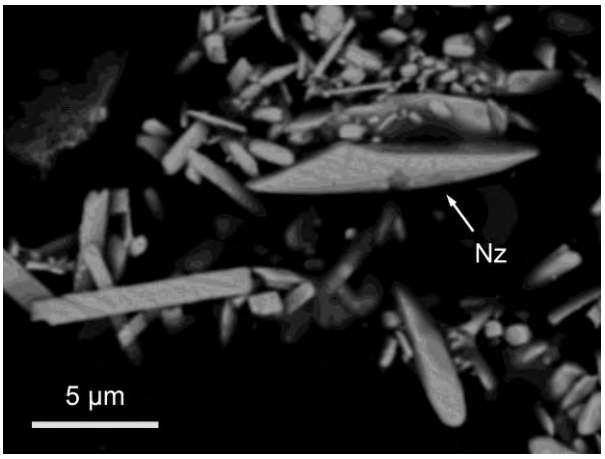

441

442 **Figure 2**

443

444

This is the peer-reviewed, final accepted version for American Mineralogist, published by the Mineralogical Society of America.
The published version is subject to change. Cite as Authors (Year) Title. American Mineralogist, in press.
DOI: https://doi.org/10.2138/am-2022-8219. http://www.minsocam.org/

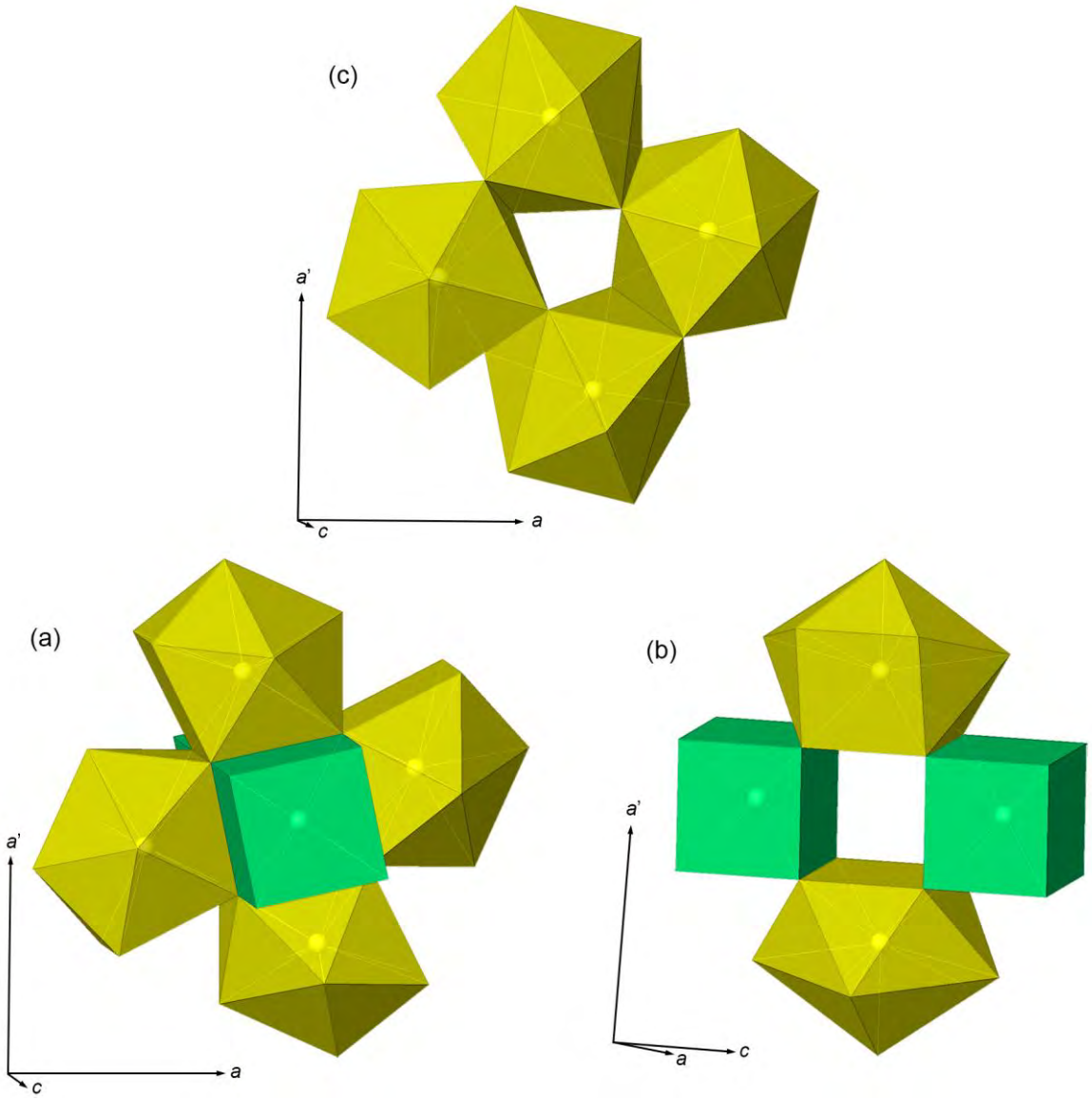

Figure 3